



Chiang Mai J. Sci. 2017; 44(2) : 630-639  
<http://epg.science.cmu.ac.th/ejournal/>  
Contributed Paper

## Bioactivity, Cytotoxicity and Antibacterial Evaluation of Undoped, Zn-doped, Sr-doped, and Zn/Sr-codoped Hydroxyapatites Synthesized by a Sol-gel Method

Likit Temprom [a], Suphasinee L. Seet [a,b,c], Patcharaporn Tippayawat [d],  
Pimsiree Suwanna\* [a,b,c,e]

[a] Materials Science and Nanotechnology Program, Faculty of Science, Khon Kaen University,  
Khon Kaen, 40002, Thailand.

[b] Intergrated Nanotechnology Research Center, Khon Kaen University, Khon Kaen, 40002, Thailand.

[c] Department of Physics, Faculty of Science, Khon Kaen University, Khon Kaen, 40002, Thailand.

[d] The center for Research & Development of Medical Diagnostic Laboratories, Faculty Associated Medical  
Sciences, Khon Kaen University, Khon Kaen, 40002, Thailand.

[e] Department of Materials Science, Faculty of Science, Kasetsart University, Bangkok, 10900, Thailand.

\*Author for correspondence; e-mail: pimsiree.s@ku.ac.th

Received: 3 April 2015

Accepted: 13 October 2015

### ABSTRACT

Undoped, Zn-doped, Sr-doped and Zn/Sr-codoped hydroxyapatite nanoparticles were synthesized using a sol-gel method. Their phases, morphologies and particle sizes were analyzed by XRD, FTIR and TEM techniques. MTT assay was performed to test cell viability against these nanoparticles. Forming ability of bonelike apatite and antibacterial activities were evaluated by immersing them in simulated body fluid (SBF) and by using agar disc diffusion assay against gram-positive *Staphylococcus epidermidis* and gram-negative *Pseudomonas aeruginosa*, respectively. The XRD and FTIR results showed the characteristic peaks of the hydroxyapatite structure; whereas the TEM results revealed nanoparticles with the size of 40-300 nm. The MTT assay indicated these nanoparticles are nontoxic. In SBF, significantly higher amount of apatite was formed on the doped-HA than on the regular HA. Incorporation of Zn ion into HA was observed to stimulate agglomeration of the newly formed apatite, whereas incorporation of Sr ion seemed to spread out the small apatite granules. Antibacterial tests demonstrated that HA alone could only inhibit the viability of *P. aeruginosa* but not *S. epidermidis*. However, its antibacterial capability against both strains was enhanced by Sr and/or Zn doping, with Sr being more effective. These doped-HA nanoparticles, therefore, could be promising candidates for future biomedical applications with good antibacterial property and apatite forming ability.

**Keywords:** hydroxyapatite, bioactivity, biocompatibility, antibacterial

## 1. INTRODUCTION

Synthetic hydroxyapatite ( $\text{HA}$ ,  $\text{Ca}_{10}(\text{PO}_4)_6(\text{OH})_2$ ) is a calcium phosphate bioceramic that has a chemical composition that is similar to that of the inorganic phase of bone and teeth. It is an attractive material for the use in biomedical applications due to its excellent biocompatibility, relatively good bioactivity and osteoconductive properties [1,2]. These properties greatly depend on particle size, morphology and chemical composition [2-4]. Nanometer-sized HA particles exhibit enhanced resorbability and much higher bioactivity due to their higher surface area for reacting with the surrounding environment in the body than their micro-sized counterparts [3,4]. The bioactivity and/or antibacterial activity of synthetic HA may also be enhanced by ionic substitutions into its crystal structure [5-16]. Among them, zinc (Zn) and strontium (Sr) are known to be biologically active ions [17].

Zn is the most abundant trace element in bone mineral. It promotes bone mineralization to induce new bone formation and is effective in inhibiting bone resorption [18]. In addition, Zn has been reported to play a special role in antimicrobial activity [8-10]. Strontium is also present in the mineral phase of bone, especially at the regions of high metabolic turn-over where new bone is regenerated [19]. Sr has also been used in a form of strontium ranelate as an antiosteoporotic agent [20]. Sr stimulates bone formation by increasing the number and activity of osteoblasts and at the same time inhibits bone resorption by reducing the number and the activity of osteoclasts.

There have been a number of studies on Zn-doped HA (ZnHA) [8-10] and Sr-doped HA (SrHA) [5-7]. Our group, however, has previously reported, for the first time, the synthesis of the Zn and Sr codoped HA nanoparticles ( $\text{ZnSrHA}$ ,  $\text{Zn}_{0.5x}\text{Sr}_{0.5x}\text{Ca}_{10-x}$

$(\text{PO}_4)_6(\text{OH})_2$ , where  $x = 0, 0.25, 0.50, 0.75$  and 1) [21]. In this work, the cytotoxicity, the ability to stimulate the formation of bonelike apatite, and the antibacterial property of the ZnSrHA nanoparticles ( $\text{Zn}_{0.5}\text{Sr}_{0.5}\text{Ca}_{10-1}(\text{PO}_4)_6(\text{OH})_2$ ) were investigated and compared to those of ZnHA, SrHA and the regular HA nanoparticles prepared using the same sol-gel procedure.

## 2. MATERIALS AND METHODS

### 2.1 Synthesis and General

#### Characterization

$\text{HA}(\text{Ca}_{10}(\text{PO}_4)_6(\text{OH})_2)$ , ZnHA ( $\text{Zn}_1\text{Ca}_{10-1}(\text{PO}_4)_6(\text{OH})_2$ ), SrHA ( $\text{Sr}_1\text{Ca}_{10-1}(\text{PO}_4)_6(\text{OH})_2$ ) and ZnSrHA ( $\text{Zn}_{0.5}\text{Sr}_{0.5}\text{Ca}_{10-1}(\text{PO}_4)_6(\text{OH})_2$ ) powders were synthesized using a previously developed sol-gel method [21]. High purity calcium nitrate tetrahydrate ( $\text{Ca}(\text{NO}_3)_2 \cdot 4\text{H}_2\text{O}$ , QRĖC), di-ammonium hydrogen phosphate,  $((\text{NH}_4)_2\text{HPO}_4$ , QRĖC), zinc acetate ( $\text{Zn}(\text{CH}_3\text{COO})_2$ , SIGMA ALDRICH) and strontium acetate ( $\text{Sr}(\text{CH}_3\text{COO})_2$ , SIGMA ALDRICH) were used as starting materials. They were mixed at the Ca+M:P mole ratio of 10:6 where M is Zn, Sr or Zn+Sr and at the Ca:M ratio of 9:1. In the case of ZnSrHA the Zn:Sr mole ratio was 1:1.

Calcium nitrate tetrahydrate was dissolved in ethanol, and when applicable the Zn and/or Sr precursors were added with the appropriate mole ratio. Di-Ammonium hydrogen phosphate was separately dissolved in deionized water. The two solutions were quickly mixed thoroughly after which the gel was formed. The gel was allowed to set in ambient temperature for 24 hours and then was heated at 80 °C until the dried powder was obtained. The dried powder was then calcined in a furnace at 600 °C for 2 hours at the heating rate of 5 °C/min and was air-cooled afterwards.

The phases of the calcined powders were

identified using X-Ray Diffraction (Expert, Panalytical, Netherlands) with  $\text{CuK}\alpha$  radiation ( $\lambda = 1.54056 \text{ \AA}$ , 30 mA, 30 kV) in the  $2\theta$  range of  $20\text{--}60^\circ$  at a scanning speed of  $0.02^\circ/\text{s}$ . The functional groups were analyzed by Fourier transform infrared (FT-IR) spectroscopy (Bruker, TENSOR 27, USA). The spectrum was recorded in the  $4000 - 400 \text{ cm}^{-1}$  region. Transmission electron microscopy (TEM) (FEI TECNAI G2 20 USA) operating at 200 kV was used to observe the morphology of the powders.

## 2.2 MTT Cytotoxicity Test

The undoped HA powder and the ZnHA, SrHA, and ZnSrHA powders were tested for their cytotoxicity by the MTT3-(4,5-dimethylthiazol-2-yl)-2,5-diphenyltetrazolium bromide) assay [22]. This assay was a modified version of conventional direct and indirect contact tests that conforms to the published standard methods (BS-EN30993-5 and ISO10993-5) using HDFn cell lines (human dermal fibroblast, neonatal, Cat.no.1IVCc-C-004-5C, Invitrogen, USA). These cells were grown in Dulbecco's Modified Eagle's Medium (DMEM) supplemented with 10% fetal bovine serum, 2 mM L-glutamine, 100 unit/ml penicillin and 100  $\mu\text{g}/\text{ml}$  streptomycin and then the cells were incubated at  $37^\circ\text{C}$  in a fully humidified, 5%  $\text{CO}_2$  air atmosphere. The test powders were dissolved in dimethyl sulfoxide (DMSO) to make a stock concentration at 10 mg/ml and then the serial dilution was made in the culture medium of cells giving 8 concentrations of 100, 50, 25, 12.5, 6.25, 3.13, 1.56 and 0.78  $\mu\text{g}/\text{ml}$ .

Human dermal skin fibroblast cells were seeded in a 96-well plate at a density of 6,000 cells/well and incubated for 48 hours. The sample at various concentrations were added to the cells and incubated for 24 hours. The test samples were removed from the cell

cultures and the cells were reincubated for a further 24 hours in fresh medium and then tested with MTT assay. Briefly, 50  $\mu\text{l}$  of MTT in PBS at 5 mg/ml was added to the medium in each well and the cells were incubated for 4 hours. Medium and MTT were then aspirated from the wells, and formazan solubilized with 200  $\mu\text{l}$  of DMSO and 25  $\mu\text{l}$  of Sorensen's Glycine buffer, pH 10.5. The optical density was read with a microplate reader (Molecular Devices) at a wavelength of 570 nm. The average of 4 wells was used to determine the mean of each point. The experiments were done 3 times to get the values of % survival of the cell lines and standard deviation. For each toxin sample, the data would be analyzed with the SoftMax Program (Molecular Devices) to determine the concentration of sample required to kill 50% ( $\text{IC}_{50}$ ) of the cells compared to that of the controls. A dose-response curve would be derived from 8 concentrations in the test range using 4 wells per concentration.

## 2.3 Bioactivity Testing (Immersion of Specimens in Simulated Body Fluid)

Ability to stimulate formation of bonelike apatite on specimen's surface can be examined by immersing the specimen in simulated body fluid (SBF). The SBF solution is prepared in accordance with the method developed by Kokubo [23]. HA, ZnHA, SrHA, and ZnSrHA powders were pressed into pellets (10-mm in diameter and 3 mm thick) and then were soaked in SBF solution and maintained at  $37^\circ\text{C}$  in the incubator for up to 4 weeks. The SBF solution was changed with a fresh one every week. At the end of week 2 and 4, one pellet of each powder composition was collected, air-dried and sputter-coated with gold. The existence and morphology of the apatite formed on the specimen's surface were observed using a scanning electron microscope (SEM) (Hitachi,

S-3000N, Japan) (HA specimen was chosen to represent the observed surface before soaking in SBF).

## 2.4 Antibacterial Activity Test

The antibacterial activity of HA, ZnHA, SrHA and ZnSrHA was tested against gram-negative *P. aeruginosa* (*Pseudomonas aeruginosa*, ATCC27803) and gram-positive *S. epidermidis* (*Staphylococcus epidermidis*, ATCC35984) by agar disk diffusion method. The organisms were prepared in sub-cultured broth at 37°C and were left overnight. After that, the solidified nutrient agar medium (Merck) was swabbed with the respective fresh microorganisms ( $1 \times 10^8$  CFU/ml). The specimen pellets (0.45 g of powder, 10 mm in diameter, pressed by 500 MPa, 120 s) were then arranged on the swabbed agar surface and incubated at 37°C for 24 hours. The results were read by measuring the diameter of the zone of inhibition (mm). The experiment was repeated four times.

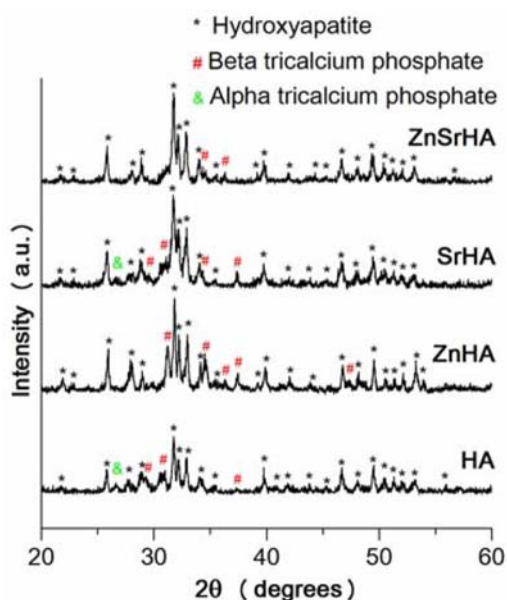


**Figure 1.** XRD patterns of HA, ZnHA, SrHA and ZnSrHA powders.

## 3. RESULTS AND DISCUSSION

### 3.1 Phase, Chemical and Morphological Characterization

The XRD patterns of the HA, ZnHA, SrHA and ZnSrHA powders are shown in Figure 1. Hydroxyapatite (JCPDs 74-0566) was found to be the main phase for all four compositions with  $\beta$ -tricalciumphosphate (JCPDs 09-0169) as a second phase. In some samples,  $\alpha$ -tricalciumphosphate (JCPDs 09-0348) was also observed. These tricalciumphosphate phases are bioceramics, which can also be used in biomedical applications [1-2]. No other crystalline phase of the doping ions was found in all samples.

The FTIR spectra of the HA, ZnHA, SrHA and ZnSrHA samples (Figure 2) show bands corresponding to the hydroxyapatite structure; that is, the characteristic bands of phosphate and hydroxyl species [3,10,13]. The band at 1087-1007  $\text{cm}^{-1}$  which is a major peak of the phosphate group corresponds to the  $\nu_3$  vibration mode. The bands at 957  $\text{cm}^{-1}$  and 556  $\text{cm}^{-1}$  belong to  $\nu_1$  and  $\nu_4$  symmetric P-O stretching vibration of the  $\text{PO}_4^{3-}$  ion, respectively. The bands corresponding to stretching modes of hydroxyl group (OH) in the hydroxyapatite can be seen at 3575  $\text{cm}^{-1}$ , 626  $\text{cm}^{-1}$  and 445  $\text{cm}^{-1}$ . In addition to the phosphate and hydroxyl groups, the bands assigned to carbonate ion,  $\text{CO}_3^{2-}$  (at 1428, 1348 and 827  $\text{cm}^{-1}$ ) and absorbed water (at 3465  $\text{cm}^{-1}$  and 1639  $\text{cm}^{-1}$ ) [3,13] are also observed in the spectra, most evidently in the spectrum for HA. The presence of  $\text{CO}_3^{2-}$  may arise from several reasons. It may result from, as suggested by Fathi et al. [3], the carbon from the organics which does not completely pyrolyze and may instead be dissolved into the hydroxyapatite crystal. It may also arise from the subsequent sample handling steps, as suggested by Stanić et al. [13]; that is the presence of Ca(II) in the surface of the

specimens may bind carbon dioxide from the air. The existence of the  $\text{CO}_3^{2-}$  bands is most pronounced for the regular HA sample and is less pronounced for the SrHA, ZnHA, and ZnSrHA samples, respectively. This may imply that incorporation of Sr and/or Zn reduces the presence of  $\text{CO}_3^{2-}$  ion in the hydroxyapatite structure.

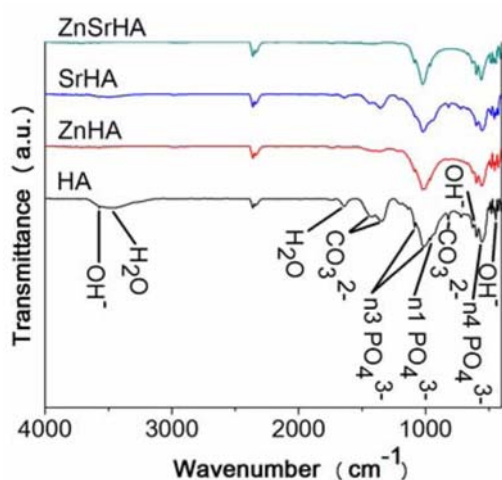


**Figure 2.** FTIR spectra of HA, ZnHA, SrHA and ZnSrHA powders.

The morphology of representative hydroxyapatite nanoparticles (HA, ZnHA, SrHA, and ZnSrHA) can be seen from the TEM images in Figure 3. In case of HA, the particles are, in general, relatively round. Most particles have the size of approximately 100-300 nm, but there are also few particles with the size of 40-100 nm. For the ZnHA, SrHA and ZnSrHA samples, both the round and rod-like particles can be seen. The size of the round particles are also in the range of 40-300 nm, but the fraction of small particles with the size of 40-100 nm is higher than that in the undoped HA. The width and the length of the rod-like particles are approximately 30-100 nm and 150-400 nm, accordingly. In this study, it is difficult to see any trend of the fractions of small round particle and the rod-like particles with

respect to the doping ions. Figure 3 also shows the selected area electron diffraction (SAED) of the HA, ZnHA, SrHA and ZnSrHA nanoparticles. It revealed that the spotty ring patterns are consistent to that of the polycrystalline HA structure (JCPDs 74-0566).

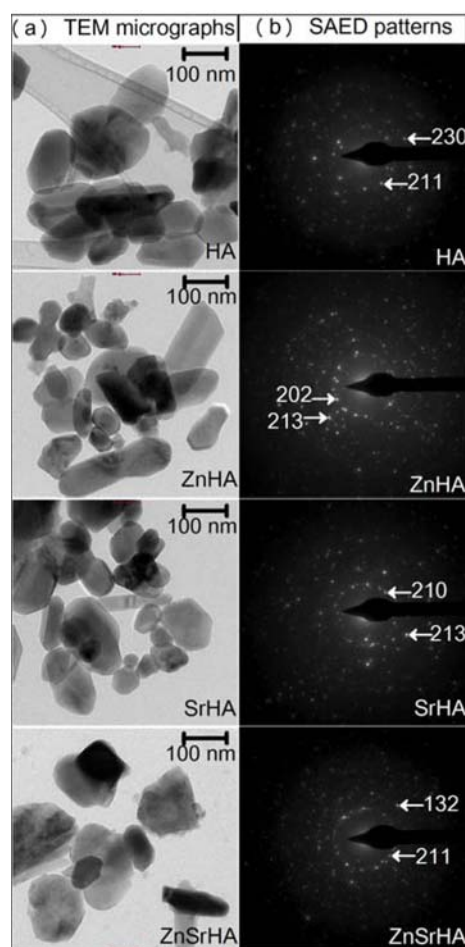


**Figure 3.** TEM micrographs of HA, ZnHA, SrHA and ZnSrHA nanoparticles and their SAED patterns.

### 3.2 Cytotoxicity Evaluation

The cytotoxicity test results for the HA, ZnHA, SrHA and ZnSrHA nanoparticles against human dermal skin fibroblast, neonatal cells (HDFn cell lines) by the MTT assay is shown in Table 1. The result is reported as

the % survival of the cells cultured with samples at concentrations of 100, 50, 25 mg/ml (results at lower concentrations are similar and hence are omitted here for brevity). The % survival of the cells in all cases are significantly higher than 50% which confirms that these HA, ZnHA, SrHA and ZnSrHA

nanoparticles are non-toxic to human dermal skin fibroblasts. It is consistent with the previous evidence indicating low cytotoxicity of ionic chemical-doped HA in both *in vitro* and *in vivo* [24]. These powders are hence expected to be biocompatible and may be used as biomaterials.

**Table 1.** The % survival of the cells cultured with samples at various concentrations and IC<sub>50</sub> value.

	Concentration (µg/ml)	Mean % Survival	Mean SD	
HA	100	93	10	
	50	93	2	>100
	25	88	6	
ZnHA	100	101	9	
	50	102	8	>100
	25	99	1	
SrHA	100	99	2	
	50	104	1	>100
	25	96	4	
ZnSrHA	100	90	5	
	50	89	7	>100
	25	87	3	

### 3.3 Apatite Forming Ability

Hydroxyapatites with different doping ions stimulate the formation of bonelike apatite from the SBF solution in a different manner. Figure 4(a) shows the surfaces of HA specimen which represent the surfaces of all specimens before soaking in SBF. Figure 4(b) shows the representative surfaces of HA, ZnHA, SrHA and ZnSrHA specimens after being immersed in the SBF for two weeks. On the HA specimen's surface, there appears only few apatite formation sites with small dimension. Significantly higher amount of apatite can be observed on the surfaces of ZnHA, SrHA and ZnSrHA specimens, however, with rather different morphology. On the surface of the SrHA, a high number of tiny apatite granules were found to spread

out over the specimen's surface and there appears to be relatively high intergranular porosity. Contradictorily, in case of the ZnHA specimen, moderate number of rather large apatite agglomerates was observed. These large agglomerates appear to be relatively dense inside and are not interconnected. A combination of these two apatite formation characteristics can be observed on the surface of the ZnSrHA specimen. Figure 4(c) shows the surface of HA, ZnHA, SrHA and ZnSrHA specimens after being immersed in the SBF for four weeks. When the specimens are immersed for longer periods in the SBF, the apatite that formed on the surface of the ZnHA, SrHA and ZnSrHA specimens were more massive, with the same characteristic previously described for each

case of doping ions. Notice that, even after four weeks, not much apatite was observed on the regular HA surface.

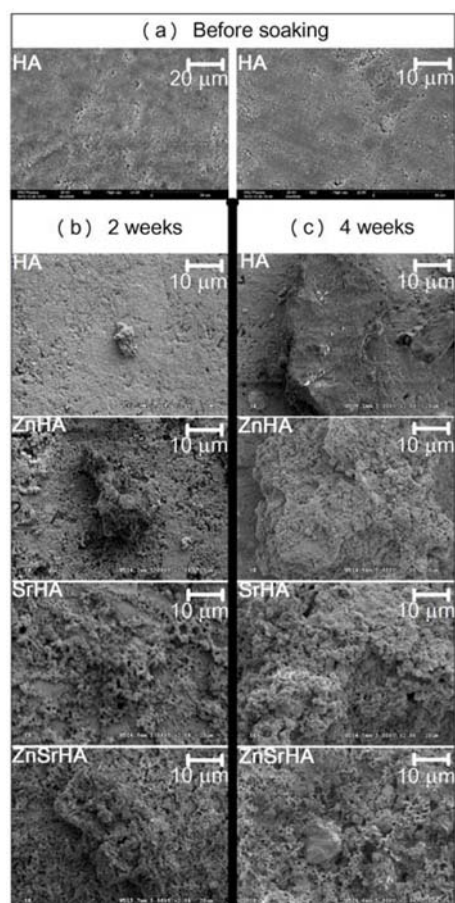


**Figure 4.** SEM micrographs of (a) HA surfaces before soaking in SBF, (b) HA, ZnHA, SrHA and ZnSrHA surfaces after soaking in SBF for 2 weeks and (c) 4 weeks.

The mechanisms of the rather different characteristics of apatite formation are still in doubt and would require further study to be identified. However, these different formation characteristics may arise from the difference in composition and structure of the specimen's surface. The ability of a preexisting surface to precipitate apatite from the SBF depends on its ability to decrease the activation barriers of the spontaneous precipitation, via heterogeneous nucleation

on specific surface sites [25,26]. This suggests that biomineralization can be induced by specific surface functional groups that act as effective sites for heterogeneous nucleation of apatite [27]. Kim *et al.* [28] have shown that during exposure to SBF, the HA of their study reveals negative charge on the surface owing to the surface hydroxyl and phosphate groups. This negative charge surface interacts with the positive calcium ions in the SBF to form a Ca-rich amorphous or nano-crystalline calcium phosphate (ACP) with positive surface charge. This Ca-rich ACP on the HA surface then interacts with the native phosphate ions in the fluid to form a Ca-poor ACP, which stabilized by being crystallized into bonelike apatite with a low solubility in the SBF. Therefore from this investigation, the specific surface functional groups acting as effective sites for heterogeneous nucleation of apatite are the hydroxyl and phosphate groups. In fact, aside from the hydroxyl and phosphate groups, different functional groups that are able to develop negative charge at the blood plasma pH have been found to be effective for calcium phosphate nucleation, e.g., carboxyl, silanol and amine groups [29-32]. The poor apatite forming ability on the undoped HA surface in this current study implies the lack of the effective surface functional groups (which may include the surface hydroxyl, phosphate and carbonate groups) that are responsible for the negative surface charge. However, incorporation of Sr modifies the presence of the effective surface functional groups of the SrHA in such a way that allows heterogeneous nucleation to simultaneously occur at numerous sites. Doping of Zn into hydroxyapatite structure, on the other hand, seems to alter the presence of the effective surface functional groups in such a way that slightly increases the nucleation sites but obviously enhances the growth and/or agglomeration of the apatite granules.

The spreading out of apatite granules on the entire surface of SrHA implies that this material may have high potential for filling the newly formed apatite in a bone defect. In addition, its relatively high intergranular porosity is expected to provide better pathways for blood vessels, living tissues and cells necessary for bone regeneration. However, the apatite layer with this morphology may have poor mechanical property; it appears to be fragile and to have relatively low strength. The denser apatite formed on the ZnHA surface is, on the other hand, expected to have higher strength and may help in preventing the propagation of a crack. However, this apatite may not provide sufficiently big pathways for bone regenerating activity to occur. In addition, with its agglomeration nature, it may not fully fill in the cavity in a defect bone. The combination of the rather dense agglomeration and the spread-out porous layer of apatite granules formed on the ZnSrHA surface may enhance its mechanical behaviors while providing sufficient pathways for bone regenerating activity.

### 3.4 Antibacterial Activities

The images of qualitative antibacterial agar disk diffusion tests are shown in Figure 5. Inhibition zones of the gram-positive *S. epidermidis* appear around the HAZn, HASr, and HAZnSr pellets, but not around the HA. This result reveals that HA alone does not inhibit the growth of *S. epidermidis*, but rather the incorporation of Zn and/or Sr into HA. The averages of the diameters of these inhibition zones are reported in Table 2. The largest average inhibition zone is observed around the SrHA pellet followed by that around the ZnSrHA and ZnHA pellets, respectively. This suggests that the doping of Sr is more effective than the doping Zn to inhibit the growth of *S. epidermidis*. In case

of the gram-negative *P. aeruginosa*, its inhibition zones can be seen around every specimen, though, with different diameters (see Table 2). This indicates that HA alone can inhibit the growth of *P. aeruginosa*. The larger inhibition zone around the SrHA pellets implies that Sr doping enhances the antibacterial activity of the HA. Zn doping, however, may not strongly synergize this activity as denoted by a smaller inhibition zone. Nevertheless, it is worth noting that all the doped HA specimen can inhibit the viability of both the gram-positive and the gram-negative strains, while the undoped HA cannot.

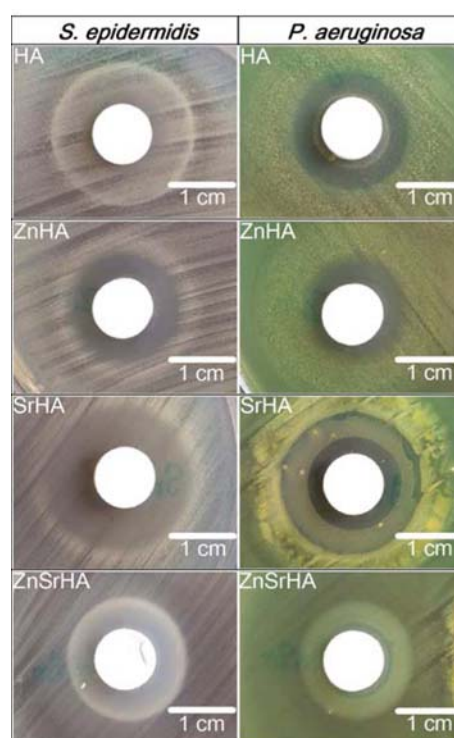


**Figure 5.** Photographs of antimicrobial test results of HA, ZnHA, SrHA and ZnSrHA tablets against *Staphylococcus epidermidis* and *Pseudomonas aeruginosa*.

The antibacterial activity of these specimens is likely due to Ca, Zn and/or Sr ions that are oxidized with oxygen in atmosphere. This oxidation reaction results

in the production of superoxide, hydrogen peroxide and hydroxyl radicals that can induce changes in the bacterial cell membrane structural constituents and finally lead to membrane damage and cell death [33-34]. From Figure 5 one can also see that the inhibition zones of the gram-positive *S. epidermidis* are not as clear as those of the gram-negative *P. aeruginosa*, which implies less capability of the specimens to inhibit the gram-positive bacteria. This is possibly due to the difference in membrane structure between the gram-positive and gram-negative bacteria; the thick negative charge of peptidoglycan of gram-positive bacterial cell membrane make it less susceptible for cationic constituent that impede the bacterial growth [35,36]. Despite their different antibacterial capability, these inorganic nanomaterials reveal the potential for controlling of microorganisms that can be beneficial for medical applications.

**Table 2.** Antibacterial efficiency of Zn and/or Sr doped HA.

Microorganism	Samples	Inhibition zone (mm)
<i>S. epidermidis</i> (gram-positive strain)	HA	-
	ZnHA	1.87±0.15
	SrHA	2.8±0.2
	ZnSrHA	1.93±0.06
<i>P. aeruginosa</i> (gram-negative strain)	HA	2.1±0.2
	ZnHA	1.57±0.21
	SrHA	2.6±0.3
	ZnSrHA	2.03±0.15

#### 4. Conclusions

As indicated by the XRD, FTIR and TEM results, the sol-gel procedure in this study can be used to synthesis hydroxyapatite nanoparticles with 10% mole Zn and/or Sr substitution for calcium. Zn and/or Sr substitutions partly modify the particle shape

and reduce the particle size and the presence of carbonate group in the hydroxyapatite structure. All specimens are not toxic to human fibroblast cell lines. In SBF, incorporation of Zn and/or Sr to HA stimulates more apatite formation. While SrHA induces many small apatite granules spreading out over the specimen's surface with high intergranular porosity, ZnHA induces much larger and denser apatite agglomerates. ZnSrHA combines these apatite formation characteristics. The undoped HA inhibits the viability of the gram-negative *P. aeruginosa* only but not the gram-positive *S. epidermidis*. All doped specimens, on the other hand, inhibit the growth of both bacteria, with the SrHA being the most effective. These doped-HA nanoparticles have different but rather interesting properties that may be adjusted for various biomedical applications.

#### ACKNOWLEDGEMENTS

This work was supported by the Higher Education Research Promotion and National Research University Project of Thailand, Office of the Higher Education Commission, through the Advanced Functional Materials Cluster of Khon Kaen University.

#### REFERENCES

- [1] LeGeros R.Z., *Clin. Orthop. Relat. Res.*, 2002; **395**: 81-98.
- [2] Vallet-Regí M. and Gonzalez-Calbet J.M., *Prog. Solid State Chem.*, 2004; **32**: 1-31.
- [3] Fathi M.H., Hanifi A. and Mortazavi V., *J. Mater. Process. Tech.*, 2008; **202**: 536-542.
- [4] Sadat-Shojai M., Khorasani M.T., Dinpanah-Khoshdargi E. and Jamshidi A., *Acta Biomater.*, 2013; **9**: 7591-7621.
- [5] Zhang W., Shen Y., Pan H., Lin K., Liu X., Darvell B.W., Lu W.W., Chang J., Deng L., Wang D. and Huang W., *Acta Biomater.*, 2011; **7**: 800-808.
- [6] Wong K.L., Wong C.T., Liu W.C., Pan

- H.B., Fong M.K., Lam W.M., Cheung W.L., Tang W.M., Chiu K.Y., Luk K.D.K. and Lu W.W., *Biomaterials*, 2009; **30**: 3810-3817.
- [7] Lin Y., Yang Z., Cheng J. and Wang L., *J. Wuhan Univ. Technol.*, 2008; **23**: 475-479.
- [8] Sutha S., Karunakaran G. and Rajendran V., *Ceram. Int.*, 2013; **39**: 5205-5212.
- [9] Chen X., Tang Q.L., Zhu Y.J., Zhu C.L. and Feng X.P., *Mater. Lett.*, 2012; **89**: 233-235.
- [10] Thian E.S., Konishi T., Kawanobe Y., Lim P.N., Choong C., Ho B. and Aizawa M., *J. Mater. Sci. Mater. Med.*, 2013; **24**: 437-445.
- [11] Cai Y., Zhang S., Zeng X., Wang Y., Qian M. and Weng W., *Thin Solid Films*, 2009; **517**: 5347-5351.
- [12] Dhal J., Bose S. and Bandyopadhyay A., *Mater. Sci. Eng. C*, 2013; **33**: 3061-3068.
- [13] Stanič V., Dimitrijevič S., Antič-Stanković J., Mitrič M., Jokič B., Plečaš I.B. and Raicevič S., *Appl. Surf. Sci.*, 2010; **256**: 6083-6089.
- [14] Shanmugam S. and Gopal B., *Appl. Surf. Sci.*, 2014; **303**: 277-281.
- [15] Fielding G.A., Roy M., Bandyopadhyay A. and Bose S., *Acta Biomater.*, 2012; **8**: 3144-3152.
- [16] Gopi D., Ramya S., Rajeswari D., Karthikeyan P. and Kavitha L., *Colloid Surface A*, 2014; **451**: 172-180.
- [17] LeGeros R.Z., *Monographs in Oral Sciences*, Basel: Karger, 1991: 1-201.
- [18] Ito A., Otsuka M., Kawamura H., Ikeuchi M., Ohgushi H., Sog Y. and Ichinose N., *Curr. Appl. Phys.*, 2005; **5**: 402-406.
- [19] Blake G.M., Zivanovic M.A., McEwan A.J. and Ackery D.M., *Eur. J. Nucl. Med.*, 1986; **12**: 447-454.
- [20] Rossi A.L., Moldovan S., Querido W., Rossi A., Werckmann J., Ersen O. and Farina M., *Micron*, 2014; **56**: 29-36.
- [21] Paennarin H. and Seet S.L., *Chiang Mai J. Sci.*, 2013; **40**: 1055-1060.
- [22] Plumb J.A., Milroy R. and Kaye S.B., *Cancer Res.*, 1989; **49**: 4435-4440.
- [23] Kokubo T. and Takadama H., *Biomaterials*, 2006; **27**: 2907-2915.
- [24] Liu Y., Sun Y., Cao C., Yang Y., Wu Y., Ju D. and Li F., *Biomaterials*, 2014; **35**: 3348-3355.
- [25] Jaakkola T., Rich J., Tirri T., Närhi T., Jokinen M., Seppälä J. and Yli-Urpo, *Biomaterials*, 2004; **25**: 575-581.
- [26] Eglín D., Maalheem S., Livage J. and Coradin T., *J. Mater. Sci. Mater. Med.*, 2006; **17**: 161-167.
- [27] Lluch A.V., Ferrer G.G. and Pradas M.M., *Polymer*, 2009; **50**: 2874-2884.
- [28] Kim H.M., Himeno T., Kokubo T. and Nakamura T., *Biomaterials*, 2005; **26**: 4366-4373.
- [29] Zainuddin, Hill D.J.T., Whittaker A.K. and Chirila T.V., *J. Mater. Sci. Mater. Med.*, 2006; **17**: 1245-1254.
- [30] Kawai T., Ohtsuki C., Kamitakahara M., Hosoya K., Tanihara M., Miyazaki T., Sakaguchi Y. and Konagaya S., *J. Mater. Sci. Mater. Med.*, 2007; **18**: 1037-1042.
- [31] Oliveira A.L., Mano J.F. and Reis R.L., *Curr. Opin. Solid St. M.*, 2003; **7**: 309-318.
- [32] Zainuddin, Hill D.J.T., Whittaker A.K., Lambert L. and Chirila T.V., *J. Mater. Sci. Mater. Med.*, 2007; **18**: 1141-1149.
- [33] Hajipour M.J., Fromm K.M., Ashkarran A.A., Aberasturi D.J., Larramendi I.R., Rojo T., Serpooshan V., Parak W.J. and Mahmoudi M., *Trends Biotechnol.*, 2012; **30**: 499-511.
- [34] Kolma J., Groszyk E. and Kwiatkowska-Rózycka D., *Biomed. Res. Int.*, 2014. DOI 10.1155/2014/178123.
- [35] Iqbal N., Kadir M.R.A., Malek N.A.N.N., Mahmood N.H.B., Murali M.R. and Kamarul T., *Mater. Res. Bull.*, 2013; **48**: 3172-3177.
- [36] Ragab H.S., Ibrahim F.A., Abdallah F., Al-Ghamdi A.A., El-Tantawy F., Radwan N. and Yakuphanoglu F., *IOSR J. Pharm. Biol. Sci.*, 2014; **9**: 77-85.